Ceramics International 48 (2022) 4686–4692

Contents lists available at ScienceDirect

Ceramics International

journal homepage: www.elsevier.com/locate/ceramint

Structural, optical and magnetic properties of Cu-doped ZrO_2 films synthesized by electrodeposition method

Rufus O. Ijeh [a,b], Cyril O. Ugwuoke [b,c], Ernest B. Ugwu [b], Samson O. Aisida [b], Fabian I. Ezema [b,d,e,f,*]

[a] Science Education Department, Collage of Education, Agbor, Nigeria
[b] Department of Physics and Astronomy, University of Nigeria, Nsukka, Enugu State, Nigeria
[c] Science and Engineering Unit, Nigerian Young Researchers Academy, 430231, Onitsha, Anambra State, Nigeria
[d] Nanosciences African Network (NANOAFNET), iThemba LABS, National Research Foundation, Somerset West, Western Cape, South Africa
[e] UNESCO-UNISA Africa Chair in Nanosciences/Nanotechnology, College of Graduate Studies, University of South Africa (UNISA), Pretoria, South Africa
[f] Africa Centre of Excellence for Sustainable Power and Energy Development (ACE-SPED), University of Nigeria, Nsukka, Nigeria

ARTICLE INFO

Keywords:
Cu-doped ZrO_2 films
Electrodeposition
Nanostructure
Optical

ABSTRACT

The electrodeposition technique was used to synthesize copper-doped ZrO_2 thin film. Different characterization technique such as vibrating sample magnetometry, UV–visible spectroscopy, scanning electron microscope, and X-ray diffractometry were used to study the magnetic, optical, surface morphology, and structural properties of the thin films. The Uniform nanocrystalline grains without cracks, and of various sizes were obtained. The optical studies showed a decrease in energy band gap from 4.1 eV to 3.9 eV. The magnetic studies revealed that the doped samples have unique ferromagnetic ordering, this could be due to the increase in grain size. The 2% and 4% doped samples are saturated around 4.51×10^{-4} emu/g and 4.70×10^{-4} emu/g at coercive field of 274.54 and 274.96 respectively.

1. Introduction

Zirconium dioxide (ZrO_2) is an essential transition metal oxide thin film of great technological importance due to its flexible nature. Zirconia exhibits high thermostability, chemical stability, high refractive index, good biocompatibility and excellent corrosion resistance which makes it a good material for medical, engineering and environmental applications [1–6]. ZrO_2 is believed to exist in three crystal phases, they include cubic (c- ZrO_2), tetragonal (t- ZrO_2), and monoclinic (m- ZrO_2). Tetragonal and cubic zirconia crystals are quite unstable at room temperature while the monoclinic zirconium crystal shows stability at room temperatures and even beyond 1170 °C [7–11]. The endearing features of ZrO_2 have made it to be one of the most promising materials for applications in solar cells, fuel cells, optical coatings, oxygen gas sensors, catalyst due to the high ion exchange capacity and as ball heads for clinical studies [12–17]. The unique properties of TiO_2 has made it significant in charge transportation and collection. However, it is used as photoelectrode in dye-sensitized solar cell (DSSC). Notwithstanding the merit, TiO_2 application as photoelectrode in DSSC is limited by its transparency and charge recombination at the interface [18,19]. Hence, it needs extra material that serves as a light reflector and as well charges separator, ZrO_2 can be conveniently used. In addition, it can be used as light absorbing layer in solar cells [20].

The deposition techniques and growth conditions of ZrO_2 are greatly influenced in structures, properties and it can as well be tailored for technological applications [21]. However, proper use of the electric field in the control of magnetism has captivated great attention because of its pertinence in the fabrication of magnetic sensor and storage devices [22–26]. These exhilarating applications impelled researchers to synthesize ZrO_2 films using various techniques which include: electron-beam evaporation [27] sol-gel [28,29], pulsed laser abrasion [30], reactive sputtering [31], ion-beam assisted deposition [32], hydrothermal [33], spray pyrolysis [34] and electron-beam [35], chemical vapour deposition [36], atomic layer deposition [37]. Among these techniques, electrodeposition is an outstanding technique because it is environmentally friendly, convenient, and capable of producing high quality materials with low-cost production appropriate for technological applications.

Studies have shown that various metals such as Tb, Au, Al, Cu, etc. have been used in doping of ZrO_2. The level of doping determines the

* Corresponding author. Department of Physics and Astronomy, University of Nigeria, Nsukka, Enugu State, Nigeria.
E-mail address: fabian.ezema@unn.edu.ng (F.I. Ezema).

https://doi.org/10.1016/j.ceramint.2021.11.004
Received 17 June 2021; Received in revised form 14 October 2021; Accepted 1 November 2021
Available online 8 November 2021

magnetic behaviour of ZrO_2 resulting in greater efficiency, higher speed, and better stability in relation to its applications [38–40]. It is important to note that Cu^{2+} ions can conveniently be doped into the ZrO_2 host lattice [41] as done in this work. Hence, the effects of Cu doping on the structural, morphological, optical, and magnetic properties of ZrO_2 was carried out. Arjun et al. studied undoped and Cu-doped ZrO_2 nanoparticles using different concentrations of copper as dopant by sol-gel approach, they observed that the crystallite size decreased as the Cu concentrations increased with morphology studies revealing spherical nanoparticles. Also, the optical analysis showed an increase in band gap values as the concentrations of Cu dopant increases [27]. Yao et al. used the radio frequency (RF) magnetron technique to synthesize Copper-doped ZrO_2 films with different Cu concentrations. They observed that the films' structure exhibited monocline (111) preferred orientation and the crystallite size increases as the concentration of Cu dopant increases. The electrical resistivity of Copper-doped ZrO_2 decreased with an increase in the concentration of Cu, this signifies the films conductivity was improved. Their values of transmittance decreased to some extent and the values of optical band gap also decreased for the copper-doped ZrO_2 films [42]. Licurgo and Paes Junior studied the effect of doping concentration on zinc oxide and the films were polycrystalline having wurtzite hexagonal structure. Also, the crystallite size increased with homogeneous nanoparticles. The optical characterization revealed that the energy band gap ranges from 3.18 to 3.27 eV which makes it feasible for optoelectronic devices [43].

In consolidation of other research works, this research is aimed to study the structural, optical and magnetic properties of undoped and Cu doped ZnO_2 thin film synthesized via electrode deposition technique, which can be conveniently used in application of solar cells.

2. Experimental details

2.1. Materials

Sodium hydroxide (NaOH), indium-doped tin oxide (ITO), zirconium (iv) oxide chloride octahydrate ($ZrOCl_2{\cdot}8H_2O$), copper sulphate pentahydrate solution ($CuSO_4{\cdot}5H_2O$), silver-silver chloride (Ag/AgCl) electrode platinum mesh.

2.2. Synthesis

The Cu-doped zirconium thin films with various doping content of Cu (0, 2, and 4 wt %) were deposited on substrates (ITO) by electrochemical deposition. The working electrodes are ITO coated substrates. The substrates were sized into 2.5 cm × 1.5 cm dimensions followed by soaking in detergent for 10 min and subsequently rinsing and ultrasonically cleaned in acetone for 30 min. The substrate was then transferred into the deposition compartment. The substrate cleaning was done to remove grease which might affect the growth and nucleation of the film. In preparing ZrO_2 nanoparticles, 70 ml of 0.3 M of zirconium (iv) oxide chloride octahydrate ($ZrOCl_2{\cdot}8H_2O$) aqueous solution and 0.9 M NaOH were mixed. The copper dopant was as well prepared by adding 2 and 4 wt % of copper sulphate pentahydrate solution ($CuSO_4{\cdot}5H_20$) in 70 ml of 0.3 M aqueous solution of zirconium (iv) oxide chloride octahydrate ($ZrOCl_2{\cdot}8H_2O$). Both solutions were mixed by stirring, while the pH was maintained at 10 by adding a precipitator agent (NaOH). The compartment is made of three-electrode systems: the anode as platinum mesh, the reference electrode as silver-silver chloride (Ag/AgCl), and the cathode as the working electrode. The working electrode was situated vertically in the chamber comprising reference and counter electrodes. The deposition was done under potentiostatic condition of 200 mV vs SCE for 10 min at room temperature followed by cleaning and drying with a hand drier. The deposited sample was taken for heat treatment using Electric Heating Thermostatic Blast Drying Oven DHG9030A (101-2) at 373 K for 1 h. The film thickness was measured by Gravimetric technique using equation (1) [44]:

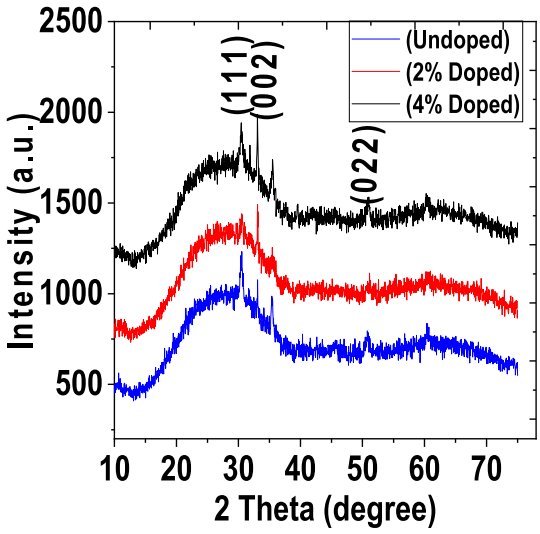

Fig. 1. XRD patterns of 0%, 2%, and 4% Cu-doped ZrO_2 thin films.

$$Thickness = \frac{mass\ difference}{(area\ of\ deposit \times density)} \quad (1)$$

0.009 g, 0.004 g, and 0.001 g were the obtained mass difference for 4%, 2%, and undoped respectively and their respective thickness are 1239.8 nm, 1115.8 nm, and 495 nm.

2.3. Characterization

Different characterization techniques were employed in studying the sample of Cu-doped zirconium dioxide. The morphological studies and the structure of undoped and Cu-doped zirconium dioxide thin films were carried out using scanning electron microscope and X-ray diffractometer (Cu Kα irradiation) respectively. The absorbance of the samples was studied using a double beam UV–vis spectrophotometer within the wavelength range of 300–1000 nm. The magnetization readings were obtained Vibrating sample magnetometry (VSM).

3. Results and discussions

3.1. Structural studies

The X-ray diffraction (XRD) patterns of the undoped and copper doped zirconium dioxide prepared using the electrodeposition method is shown in Fig. 1. From the result, it was confirmed that all the electrodeposited samples exhibit crystalline peaks at (111), (002) and (022) planes corresponding to monoclinic ZrO_2. The peak positions of undoped and doped zirconium dioxide thin films were observed to be almost the same as the atomic radii of zirconium and copper are (0.80 Å) and copper (0.72 Å) respectively. This result is in consonance with the works of Arjun et al. [32]. The incorporation of Copper into Zr atoms results in the decrease of energy band gap. At the diffraction peak (111) which is dominant, the grain sizes of ZrO_2 nanocrystalline films were calculated from the full width at half maximum (FWHM) using Debye Schrerrer's formula [45–47].

$$D = \frac{k\lambda}{\beta Cos\theta} \quad (2)$$

where D is the grain size, λ is the wavelength of X-ray (CuKα radiation λ = 1.5405 Å), K = 0.9 which is the correction factor, β is FWHM of the most intense diffraction factor, and θ is the Bragg angle. The crystallite size of undoped, 2 and 4 % wt. doped of doped ZrO_2 thin films were calculated to be 9.8, 10.0 and 10.3 nm respectively and this is

Table 1
The calculated values of crystallite size and FWHM.

Sample	Grain size D(nm)	FWHM (degree)
Undoped ZrO_2	3.88	0.2058
2% Doped	3.93	0.2029
4% Doped	3.97	0.2015

summarized in Table 1. The result confirms that the particle size of undoped zirconium dioxide is higher than the doped samples. This can be attributed to the constraint of the motion of crystallites at the interaction between host and dopant crystallites due to stress formation [48]. This result is similar to the works of Singh & Nakate that obtained the calculated crystallite size to be 8.8 nm [49,50].

3.2. Morphological studies

The morphological studies of zirconium dioxide thin films were investigated using a scanning electron microscope (SEM). The SEM images showing the effect of doping in the ZrO_2 samples are displayed in Fig. 2(a–c). From the micrographs, it is observed that the deposited films are quite homogenous over the entire surface, spherical aggregates, dense and without any void. This is because the grains are firmly stocked onto the substrate as presented in Fig. 2(b and c). Among the doping contents, it is observed that the 4% doped sample has larger grains that are cross-linked, having the same magnification of 100×. The trend in the variation of grain size is in good agreement with the work of Nian-Qi et al. [51]. There is evidence of aggregate of smaller grains that resulted in larger sizes which might be the effect arising from the particles nucleation on the substrate.

3.3. Optical studies

3.3.1. Optical transmittance and absorbance

The UV–visible spectrophotometer was used to study the transmittance spectra of Cu-doped ZrO_2 within the spectra region at the wavelength range of 300–1000 nm. Fig. 3 shows the transmittance spectra of the samples. It was noted that as the thin films exhibited continuous transmittance across the UV–vis spectrum which decreases near the UV region. From the transmittance spectrum, the undoped thin films recorded a high transmittance value of 66.8% at 450 nm and remained fairly constant in the visible region whereas the 2% and 4% Cu-doped samples have a low transmittance value of 26.5% and 25.9% respectively. At 750 nm, the undoped transmitted at 68% whereas the 2% and 4% doped samples have high transmittance values of 65.5% and 64.9% respectively. The obtained high values of transmittance suggest that ZrO_2 can excellently be used for transparent electronic applications. This result is in harmony with the works of Ortiz et al. whose transmittance value was about 80% calcined at 550 °C and 575 °C [36]. This result is also congruent with the works of Yao et al. whose average transmittance value decreased from 88.46% to 83.11% as the percentage of Cu dopant increased [37]. The decrease in the transmittance value of the doped ZrO_2 films may be due to defects of ZrO_2 or the incident photons that are scattered by the metallic Cu crystals residing at ZrO_2 lattice [50,51].

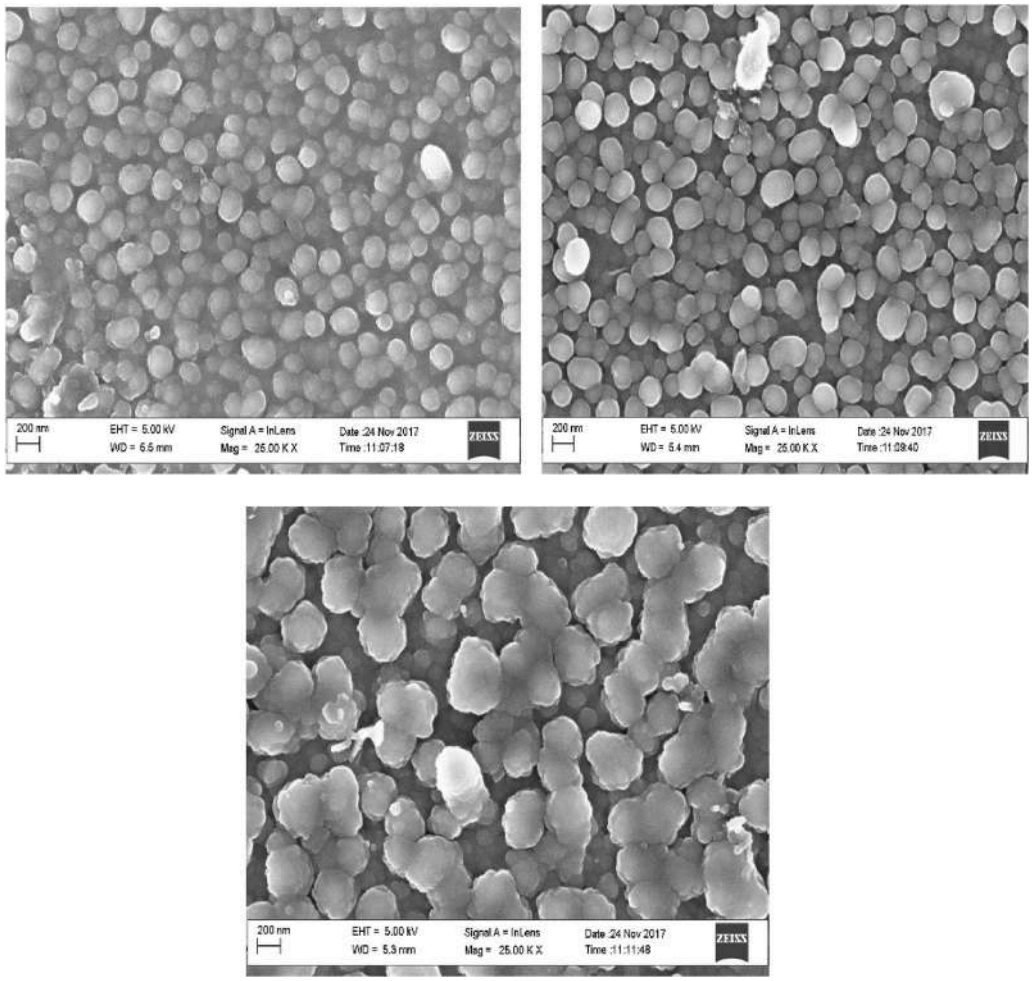

Fig. 2. SEM micrograph of (a) undoped ZrO_2 (b) 2% doped ZrO_2 thin films and (c) 4% doped ZrO_2 thin films.

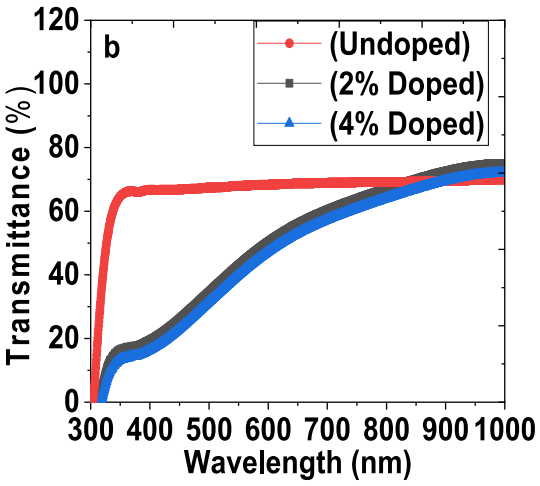

Fig. 3. The plots of Transmittance spectra for the undoped and Cu-doped ZrO_2 thin films.

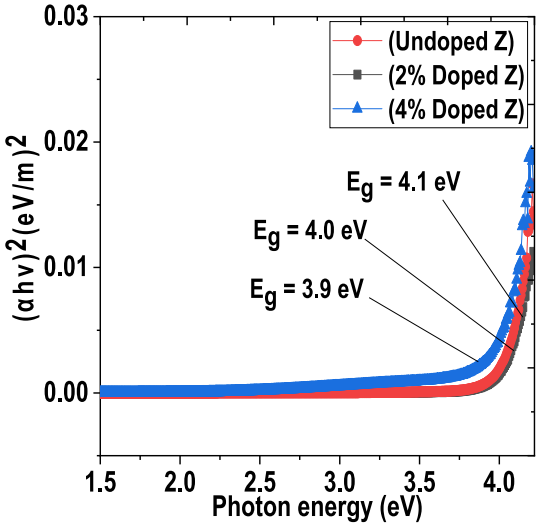

Fig. 4. Optical band gap plots for undoped and doped samples.

3.3.2. *Optical bandgap*

The band gap of thin films is best determined by the absorption coefficient (α). Fig. 4 depict the measurement of the absorption coefficient relative to the photon energy (hν). The optical band gap (Eg) of the samples are obtained by the plot of absorption coefficient against the photon energy. This can be effectively determined using the following relation [52]:

$$(\propto hv)^{1/2} = = A(hv - Eg) \tag{3}$$

where Eg is the energy band gap, ∝ is the absorption coefficient, A is a proportionality constant, h is Planck's constant, and n is the photon energy. The linear plot gave the energy band gap values for the undoped, 2% and 4% doped samples as 4.1, 4.0 and 3.9 eV respectively. This imports that the increase in doping percentage results in a reduction of the band gap hence, causing a redshift of the optical absorption edge. This work is in compromise with that of Hussain et al. whose bandgap decreased from 4.31 to 3.7 eV when zirconium dioxide was doped with cobalt [53]. This work is also in conformity with the works of Nian-Qi et al. whose energy bandgap values reduced from 4.64 to 4.61 eV when copper was doped with zirconium dioxide [51]. This work is also in agreement with the works of Pramanik et al. they noted that the band gap decreases from 4.30 to 3.48 eV when copper was doped with

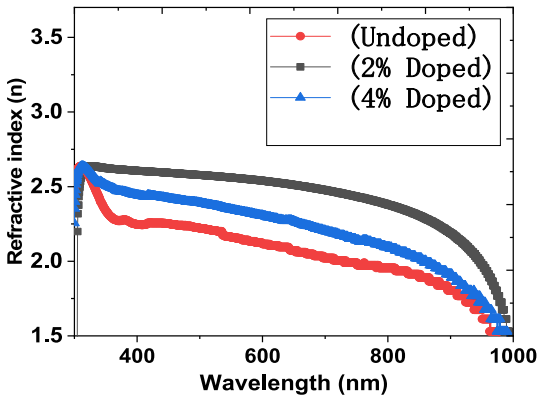

Fig. 5. Plot of refractive index versus wavelength of the undoped and doped ZrO_2 thin films.

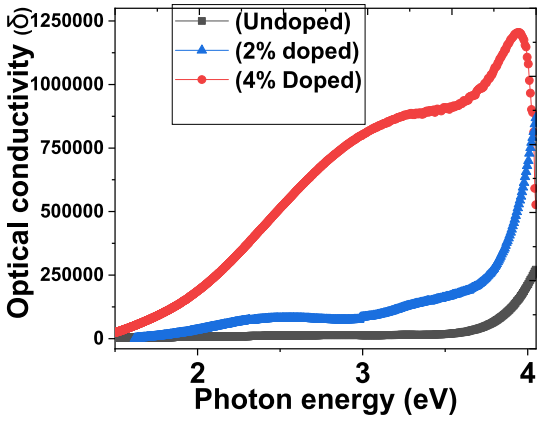

Fig. 6. The plot of optical conductivity of undoped and doped ZrO_2 thin films.

zirconium [54]. The reduction in band gap as the percentage of the doping increases could be due to the increase in electron density forming a donor level below the conduction band.

3.3.3. *Refractive index*

Fig. 5 presents the variation of refractive index with wavelength for undoped and Cu-doped ZrO_2 thin films. Generally, optical properties vary with wavelengths of light. Therefore, it becomes imperative to understand their dependence within the range of wavelengths of 300–1000 nm [55]. The values of refractive index for undoped and doped were obtained using Eq. (4) [56]:

$$\eta = \frac{1 + \sqrt{R}}{1 - \sqrt{R}} \tag{4}$$

where R is the reflectance and n is the refractive index.

The refractive indices, n of both doped and undoped samples decreased with the increase in wavelength. This is due to the decrease in absorbance and increase in transmittance values as wavelength increases [57]. At 800 nm, while the undoped refracted at 1.9, the 2 and 4% doped thin films are refracted at 2.3 and 2.0 respectively. This might be due to surface and volume imperfections as photon energies were trapped [58]. This result is consistent with the works of Hojabri that had a refractive index ranging from 2.10 to 2.25 [59].

3.3.4. *Optical conductivity*

The disparity of optical conductivity in relation to the photon energy for both undoped and copper doped ZrO_2 is shown in Fig. 6 and this can be calculated using Eq. (5) [60,61]:

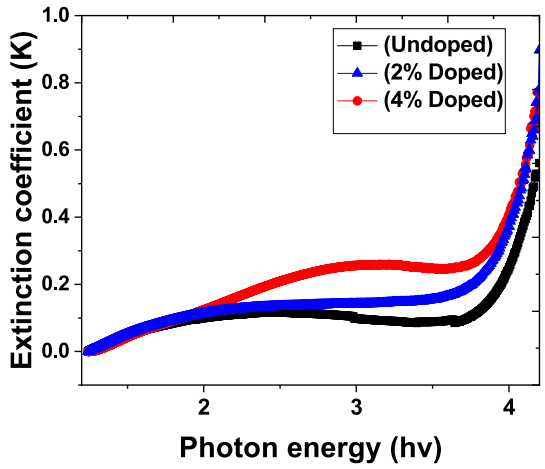

Fig. 7. Extinction coefficient plot of undoped and copper doped ZrO_2 thin films.

$$\delta = \frac{\alpha n c}{4\pi} \tag{5}$$

where α is the absorption coefficient, n is the refractive index, and c is the speed of light. The presence of low energy density resulted in the highest resistivity exhibited by the undoped sample. It is evident that the introduction of copper dopant is active, thereby resulting in the increase in the films electrical conductivity as shown in Fig. 6. Among the samples, the 4% doped sample had a sharp increase in conductivity. This, however, may be ascribed to the formation of the new doping levels in the band gap caused by the Cu doping. The undoped sample had very low conductivity at both low and high photon energies due to the absence of carrier concentration. This result is in agreement with the works of Licurgo et al. the electrical conductivity of ZnO thin films increases when the Cu doping concentration increases [62].

3.3.5. Extinct coefficient

At a given wavelength, the degree of attenuation of light into a sample can be measured using the extinction coefficient. This can be estimated using the relation [63]:

$$K = \frac{\alpha\lambda}{4\pi} \tag{6}$$

where α is the absorption coefficient, k is the extinction coefficient, and λ is the wavelength of the incident photons. From eq. (6) it is noted that as the absorption coefficient increases, the extinction coefficient also increases. It is as well observed that the undoped and 2% doped samples have an extinction coefficient of 0.09 and 0.14 respectively, whereas the 4% doped sample recorded the highest extinction coefficient of 0.26 as shown in Fig. 7. This result is in agreement with the works of Shanmuganathan et al. as the values of extinction coefficients ranged between 0.001 and 0.0163 when ZnO was doped with potassium [64]. It is expedient to say that all samples showed a low extinction coefficient for the entire photon energy. This might be due to the smoothness and the homogeneity of the samples [65].

3.3.6. Dielectric constants

The dielectric constant in a given material comprises the real and the imaginary parts. The imaginary dielectric constant (ε_i) describes the energy absorption from the electric field while the real part (ε_r) is concerned with property hampering the speed of light in the material [66]. The electronic properties of materials are best determine using the dielectric constant [67,68]. The imaginary (ε_i) and the real parts (ε_r) complex dielectric constants were determined from the refractive index and the extinction coefficient using the following equations [68].

$$\varepsilon_r = n^2 - k^2 \tag{7}$$

$$\varepsilon_i = 2nk \tag{8}$$

The variations in real and imaginary dielectric constants in relation to the photon energy for both doped and undoped samples are presented in Fig. 8. The imaginary values are lower than the real values although both values increase slightly with doping concentration. At lower photon energy, the imaginary part shows a very sharp increase and was observed to shrink at higher energy. The real and imaginary parts show the relaxation peaks at 4.1 and 1.2 respectively.

4. Magnetic properties

The VSM was used to study the magnetic properties of undoped and copper doped ZrO_2 thin films. The spin interactions which take place in magnetic domains between Cu and ZrO_2 result in exchange-coupling and this allow spontaneous magnetization [69]. The hysteresis loop was observed in both doped and undoped ZrO_2 thin films. It is plausible to say that changes in the electron density of samples affect the ferromagnetic properties which lead to the shift in Fermi level upon introduction of the electric field [70–73]. The field-dependent magnetization (M − H) curves were recorded in the range of ±400 kOe at room temperature as shown in Fig. 9. The Cu doped and undoped samples shows ferromagnetic properties. The ferromagnetic behavior of the undoped

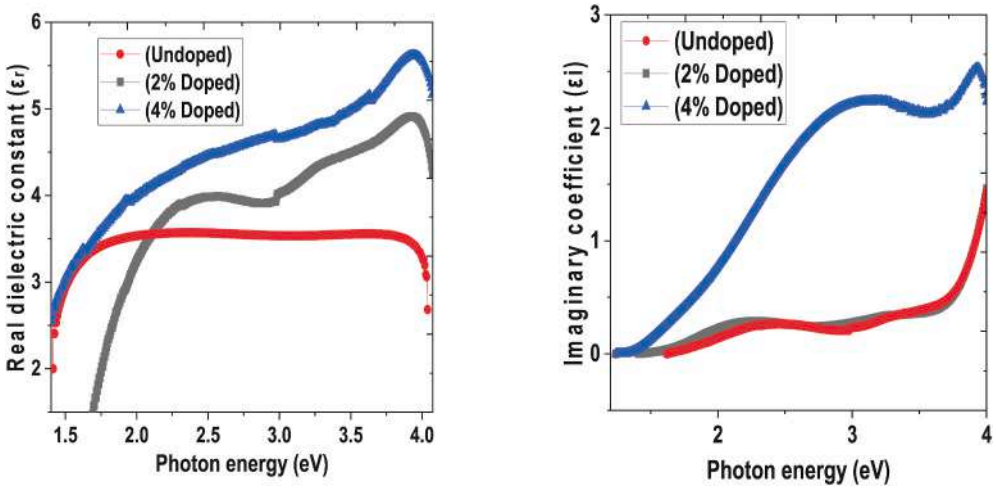

Fig. 8. The plot of dielectric constants of undoped and doped ZrO_2 thin films.

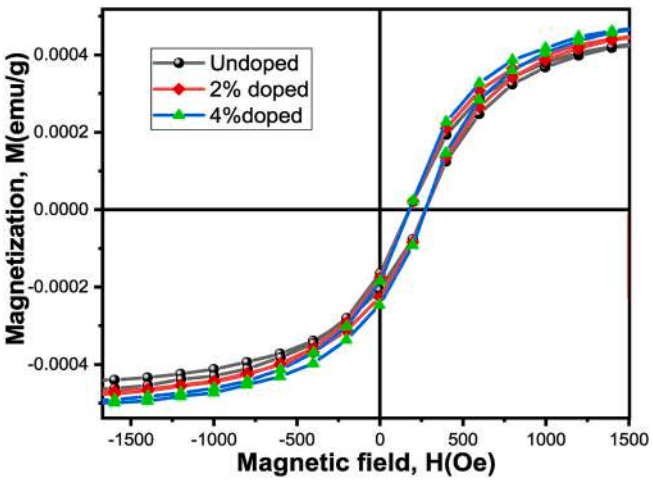

Fig. 9. Magnetic curves of (a) Undoped and (b) Cu-doped ZrO_2 thin films.

Table 2
The magnetization of undoped and Cu-doped ZrO_2 thin films.

Samples	Magnetic saturation (M_s) (emu/g)	Remnance magnetization (M_r) (emu/g)	Coercive field (H_c) (O_e)
Undoped	4.34×10^{-4}	2.06×10^{-4}	273.69
2% Doped	4.51×10^{-4}	2.30×10^{-4}	274.54
4% Doped	4.70×10^{-4}	2.47×10^{-4}	274.96

sample might be due the defects of oxygen vacancies. In this work, the coercive field and the remnance magnetization for the doped samples were observed to increase as the Cu doping percentage increases. However, it is plausible to say that doped samples exhibited higher magnetizations than the undoped due increase in grain size, this has the propensity of increasing the magnetic ordering [74,75]. This work agrees with the works of Kumar et al., Shah et al. and Gopalakrishnan et al. [76–78] which support the idea that the introduction of impurities and procedure of measurements enhances magnetization. The magnetization of the undoped sample is saturated around 4.34×10^{-4} emu/g at high coercive field of 273.69, whereas the 2% and 4% doped samples are saturated around 4.51×10^{-4} emu/g and 4.70×10^{-4} emu/g at coercive field of 274.54 and 274.96 respectively as depicted in Table 2. More so, the 2% doped sample shows the range of magnetic field from 4.51×10^{-4} to -4.75×10^{-4} whereas that of 4% doped sample ranges from 4.70×10^{-4} to -4.95×10^{-4}.

5. Conclusion

The undoped and Cu-doped ZrO_2 thin films were grown by the electrodeposition technique for this study. The X-ray diffraction, UV–visible spectroscopy, Vibrating sample magnetometry, and Scanning Electron Microscopy techniques were utilized in this study. The structural analysis revealed that both undoped and doped samples were found to be monoclinic in nature with morphology being uniform, spherical and without crack. The undoped sample transmittance was observed to be 68% whereas the 2% and 4% doped samples were 65.5% and 64.9% at 750 nm respectively. It was observed the band gap energy decreases from 4.1 eV to 3.9 eV as the doping percentage increases and the magnetic property of the samples were observed to increase as the doping percentage increases.

Declaration of competing interest

The authors declare that they have no known competing financial interests or personal relationships that could have appeared to influence the work reported in this paper.

Acknowledgements

FIE acknowledges the grant by TETFUND under contract number TETFUND/DR&D/CE/UNI/NSUKKA/RP/VOL.I and also acknowledges the support received from the Africa Centre of Excellence for Sustainable Power and Energy Development (ACE-SPED), University of Nigeria, Nsukka.

We thank Engr. Emeka Okwuosa for the generous sponsorship of April 2014, July 2016, July 2018 and July 2021 conferences/workshops on applications of nanotechnology to energy, health &. Environment and for providing some research facilities.

References

[1] A. Hirvonen, R. Nowak, Y. Yamamoto, T. Sekino, K. Niihara, Fabrication, structure, mechanical and thermal properties of zirconia-based ceramic nanocomposites, J. Eur. Ceram. Soc. 26 (8) (2006) 1497–1505.
[2] J.C. Ray, D. Park, W.S. Ahn, Chemical synthesis of stabilized nanocrystalline zirconia powders, J. Ind. Eng. Chem. 12 (1) (2006) 142–148.
[3] K.W. Xu, S. Zhao, F. Ma, Z.X. Song, Thickness-dependent structural and optical properties of sputter deposited ZrO_2 film, Opt. Mater. 30 (2008) 910–915.
[4] C.Y. Ma, F. Laspostolle, P. Briois, Q.Y. Zhang, Effect of O_2 gas partial pressure on structures and dielectric characteristics of rf sputtered ZrO2 thin films, Appl. Surf. Sci. 253 (2007) 8718.
[5] Y. Shen, S. Shao, H. Yu, Z. Fan, H. He, J. Shao, Influences of oxygen partial pressure on structure and related properties of ZrO2 thin films prepared by electron beam evaporation deposition, Appl. Surf. Sci. 254 (2007) 552.
[6] R.F. Laidan, N. Gottardi, G. Micheli, V. Bartali, R. Jestin, Y. Tomasella, E. Ferrari, M. Thomas, Investigation of structural and optical properties of sputtered zirconia thin films, Eur. Phys. *J. Appl. Phys.* 43 (2008) 363.
[7] W. Cao, J. Kang, G. Fan, L. Yang, F. Li, Fabrication of porous ZrO_2 nanostructures with controlled crystalline phases and structures via a facile and cost-effective hydrothermal approach, Ind. Eng. Chem. Res. 54 (51) (2015) 12795–12804.
[8] G.N. Shao, S.M. Imran, S.J. Jeon, M. Engole, N. Abbas, S.M. Haider, S.J. Kang, H. T. Kim, Sol–gel synthesis of photoactive zirconia–titania from metal salts and investigation of their photocatalytic properties in the photodegradation of methylene blue, Powder Technol. 258 (2014) 99–109.
[9] N. Yao, Z. Liu, G. Gu, B. Wu, Structural, optical, and electrical properties of Cu-doped ZrO_2 films prepared by magnetron co-sputtering, *Chin. Phys.* B 26 (10) (2017) 106801.
[10] Z.W. Zhao, B.K. Tay, G.Q. Yu, S.P. Lau, Optical properties of filtered cathodic vacuum arc-deposited zirconium oxide thin films, J. Phys. Condens. Matter 15 (2003) 7707–7716.
[11] C. Kuranaga, R. Leite, M. Filgueira, Toughened RE-TZP ceramics obtained by HPHT process, 196, J. Mater. Process. Technol. 21 (1–3) (2008) 373–378.
[12] W. Li, X. Liu, A. Huang, P. Chu, Structure and properties of zirconia (ZrO_2) films fabricated by plasma-assisted cathodic arc deposition, J. Phys. D Appl. Phys. 40 (2007) 2293–2299, https://doi.org/10.1088/0022-3727/40/8/S08.
[13] V.G. Zavodinsky, The mechanism of ionic conductivity in stabilized cubic zirconia, Phys. Solid State 46 (3) (2004) 453–457.
[14] J. Riegel, H. Neumann, H. Wiedenmann, Exhaust gas sensors for automotive emission control, Solid State Ionics 153 (2002) 783–800.
[15] J.C. Garcia, L.M. Scolfaro, A.T. Lino, Structural, electronic, and optical properties of ZrO_2 from abinitio calculations, J. Appl. Phys. 100 (10) (2006). Article ID 104103.
[16] S. Park, J.M. Vohs, R.J. Gorte, Direct oxidation of hydrocarbons in a solid-oxide fuel cell, Nature 404 (6775) (2000) 265–267.
[17] H. Subbarao, S. Maiti, Science and technology of zirconia, Adv. Ceram. 24 (1988) 731–737.
[18] C.O. Ugwuoke, S. Ezugwu, S.L. Mammah, A.B.C. Ekwealor, M. Suguyima, F. I. Ezema, Physical Methods to Fabricate TiO2 QDs for Optoelectronics Applications, in: Electrode Materials in Energy Storage and Conversion, 2021, pp. 321–338.
[19] K.S. Pawar, P.K. Baviskar, I. Altafhusain, B.N. Sunita, S. Gawali, Layer-by-layer deposition of TiO_2–ZrO_2 electrode sensitized with Pandan leaves : natural dye-sensitized solar cell, Mater. Renew. Sustain. Energy 8 (2) (2019) 1–9, https://doi.org/10.1007/s40243-019-0148-x.
[20] E. Sani, L. Mercatelli, J. Sans, D. Sciti, Optical properties of black and white ZrO 2 for solar receiver applications, Sol. Energy Mater. Sol. Cells (2015) 1–6, https://doi.org/10.1016/j.solmat.2015.02.007.
[21] W. Prellier, A. Fouchet, B. Mercey, Oxide-diluted magnetic semiconductors: a review of the experimental status, J. Phys. Condens. Matter 15 (2003) 37.
[22] S.A. Chambers, T.C. Droubay, C.M. Wangl, Ferromagnetism in oxide semiconductors, Mater. Today 9 (11) (2006) 28–35.
[23] C. Barraud, C. Deranlot, P. Seneor, Magnetoresistance in magnetic tunnel junctions grown on flexible organic substrates, Appl. Phys. Lett. 96 (7) (2010) 911.

[24] M. Melzer, G. Lin, D. Makarov, Stretchable spin valves on elastomer membranes by predetermined periodic fracture and random wrinkling, Adv. Mater. 24 (48) (2012) 6468.

[25] P. Sheng, B. Wang, R. Li, Flexible magnetic thin films and devices, J. Semiconduct. 39 (2018) 1.

[26] A. Arjun, A. Dharr, T. Raguram, and K. S. Rajni, "Study of copper doped zirconium dioxide nanoparticles synthesized via sol–gel technique for photocatalytic applications," J. Inorg. Organomet. Polym. Mater., doi:10.1007/s10904-020-01616-4.

[27] S. Asadi, H. Abdizadeh, Y. Vahidshad, Effect of crystalline size on the structure of copper doped zirconia nanopaticles synthesized via sol-gel, J. Nanostruct. 2 (2012) 208–212, 02.008.

[28] S. Park, G.N. Shao, Microstructure and materials characterization of sol-gel synthesized ZrO_2, Tanzan. J. Sci. 45 (2) (2019) 190–208.

[29] A.O. Dikovska, G.B. Atanasova, G.V. Avdeev, V.Y. Strijkova, Thin nanocrystalline zirconia films prepared by pulsed laser deposition, J. Phys. Conf. 700 (2016), 012024.

[30] M. Matsuoka, S. Isotani, J.F. Chubaci, Influence of ion energy and arrival rate on x-ray crystallographic properties of thin ZrO x films prepared on Si (111) substrate by ion-beam assisted deposition, J. Appl. Phys. 88 (6) (2000) 3773–3775.

[31] A. Keiteb, E. Saion, A. Zakaria, N. Soltani, Structural and Optical Properties of Zirconia Nanoparticles by Thermal Treatment Synthesis" Journal of Nanomaterials, 2016, pp. 1–6, https://doi.org/10.1155/2016/1913609.

[32] G. Sethi, P. Sunal, M. Horn, M. Lanagan, Influence of reactive sputter deposition conditions on crystallization of zirconium oxide thin films, J. Vac. Sci. Technol. A Vac. Surf. Film 27 (3) (2009) 577.

[33] D. Neumayer, E. Cartier, Materials characterization of ZrO_2-SiO_2 and HfO_2-SiO_2 binary oxides deposited by chemical solution deposition, J. Appl. Phys. 90 (4) (2001) 1801–1808.

[34] N.Q. Yao, Z.C. Liu, G.R. Gu, B.J. Wu, Structural, optical, and electrical properties of Cu- doped ZrO_2 films prepared by magnetron co-sputtering, Chin. Phys. *B* 26 (10) (2017), 106801, https://doi.org/10.1088/1674-1056/26/10/106801.

[35] l. Kraus, O. Chayka, A.C hysteresis loop tracer for soft magnetic thin films, J. Electr. Eng. 57 (8/S) (2006) 73–76.

[36] S. Selvaraj, J. Parulekar, Selective atomic layer deposition of zirconia on copper patterned silicon substrates using ethanol as oxygen source as well as copper reductant, J. Vac. Sci. Technol. 32 (2014), 010601, https://doi.org/10.1116/1.4826941.

[37] A. Ortiz, J. Alonso, E. Haro-Poniatowski, Spray deposition and characterization of zirconium-oxide thin films, J. Electron. Mater. 34 (2) (2005) 150–155, https://doi.org/10.1007/s11664-005-0226-y.

[38] R.O. Ijeh, A.C. Nwanya, A.C. Nkele, I.G. Madib, A.K. Bashir, A.B.C. Ekwealor, R. U. Osuji, M. Maaza, F.I. Ezema, "Optical, electrical and magnetic properties of copper doped electrodeposited MoO_3 thin films, Ceram. Int. 46 (8) (2020) 10820–10828.

[39] P.K. Sharma, R.K. Dutta, A.C. Pandey, S. Layek, H.C. Verma, Effect of iron doping concentration on magnetic properties of ZnO nanoparticles, J. Magn. Magn Mater. 321 (17) (2009) 2587–2591.

[40] R. Septawendar, A. Nuruddin, S. Sutardi, E. Maryani, A.T. Lia, W. Asri, S. B. Purwasasmita, Low-temperature metastable tetragonal zirconia nanoparticles (NpMTZ) synthesized from local zircon by a modified sodium carbonate sintering method, J. Austr. Ceram. Soc. 54 (2018) 643–654.

[41] N. Scotti, F. Bossola, F. Zaccheria, N. Ravasio, Copper-zirconia catalysts: powerful multifunctional catalytic tools to approach sustainable process, Catalyst 10 (2) (2020) 168, https://doi.org/10.3390/catal10020168.

[42] J.S. Licurgo, H.R. Paes Junior, Morphological, structural, electrical and optical properties of copper-doped zinc oxide films deposited by spray pyrolysis, Mater. Sci. Forum 930 (2018) 79–84. https://doi.org/10.4028/www.scientific.net/msf.930.79.

[43] T.F. Paes, A.F. Beloto, E.C. de, S. Galvão, L.A. Berni, Simple method for measuring the porosity, thickness and refractive index of porous silicon, based on the Fabry-Pérot interference spectrum, Revista Brasileira de Aplicações de Vácuo 35 (2017) 117–122, https://doi.org/10.17563/rbav.v35i3.1044.

[44] S. Tanemura, L. Miao, P. Jin, K. Kaneko, A. Terai, N. Nabatova-Gabain, Optical properties of polycrystalline and epitaxial anatase and rutile TiO_2 thin films by rf magnetron sputtering, Appl. Surf. Sci. 212–213 (2003) 654–660.

[45] D. Smilgies, Scherrer grain-size analysis adapted to grazing-incidence scattering with area detectors, J. Appl. Crystallogr. 42 (2009) 1030–1034, https://doi.org/10.1107/S0021889809040126.

[46] A.O. Bokuniaeva, A. S Vorokh, Estimation of particle size using the Debye equation and the Scherrer formula for polyphasic TiO_2 powder, J. Phys. Conf. (2019) 1410, https://doi.org/10.1088/1742-6596/1410/1/012057.

[47] A.K. Singh, U.T. Nakate, Microwave synthesis, characterization, and photoluminescence properties of nanocrystalline zirconia, Sci. World J. (2014), https://doi.org/10.1155/2014/349457.

[48] B. Cojocaru, D. Avram, V. Kessler, V. Parvulescu, G. Seisen-baeva, C. Tiseanu, Nanoscale insights into doping behavior, particle size and surface effects in trivalent metal doped SnO_2, Sci. Rep. 7 (2017) 9598.

[49] E.S. Agorku, A.T. Kuvarega, B.B. Mamba, A.C. Pandey, A.K. Mishra, Enhanced visible light photocatalytic activity of multielements-doped ZrO_2 for degradation of indigo carmine, J. Rare Earths 33 (5) (2015) 498.

[50] N.L. Tarwal, K.V. Gurav, S.H. Mujawar, S.B. Sadale, K.W. Nam, W.R. Bae, Photoluminescence and photoelectrochemical properties of the spray deposited copper doped zinc oxide thin films, Ceram. Int. 40 (6) (2014) 7669–7677.

[51] N. Yao, Z. Liu, G. Gu, B. Wu, Structural, optical, and electrical properties of Cu-doped ZrO_2 films prepared by magnetron co- sputtering, Chin. Phys. 26 (10) (2017) 106801, https://doi.org/10.1088/1674-1056/26/10/106801.

[52] F. Rebib, N. Laidani, G. Gottardi, V. Micheli, R. Bartali, Y. Jestin, E. Tomasella, Investigation of structural and optical properties of sputtered Zirconia thin films, Phys. J. 368 (2008) 363–368.

[53] S.A. Hussain, A.H. Omran, A. lkhayatt, E.A. Mahdi, Effect of Co-Dopant on the structural and optical properties of nanocrystalline ZrO_2 thin films prepared by spray pyrolysis technique, J. Appl. Phys. 8 (5) (2016) 44–49.

[54] P. Pramanik, S. Singh, D.C. Joshi, A. Mallick, Cubic phase stability , optical and magnetic properties of Cu-stabilized zirconia nanocrystals, J. Phys. D Appl. Phys. 51 (12pp) (2018) 225304, https://doi.org/10.1088/1361-6463/aac004.

[55] A.R. Forouhi, I. Bloomer, Optical dispersion relations for amorphous semiconductors and amorphous dielectrics, Phys. Rev. B 34 (1986) 7018–7026, https://doi.org/10.1590/1516-1439.039215, 1000-1007.

[56] T.S. Moss, G.J. Burrell, B. Ellis, Semiconductor Optoelectronics, Butterworths, London, 1973, pp. 874–875.

[57] P. Ambika, B. Barman, An optical study of vacuum evaporated Se85-xTe15Bix chalcogenide thin films, Physica B 405 (2010) 822.

[58] H.C. Ong, J.Y. Dai, K.C. Hung, Y.C. Chan, S.T. Ho, Electronic Structures of Polycrystalline ZnO thin films probed by electron energy loss spectroscopy, *Appl. Phys.* Lett. 77 (10) (2000) 1484.

[59] A. Hojabri, Structural and optical characterization of ZrO_2 thin films grown on silicon and quartz substrates, J. Theor. Appl. Phys. 10 (3) (2016) 219–224.

[60] H.S. Bolarinwa, M.U. Onuu, A.Y. Fasasi, S.O. Alayande, L.O. Animasahun, I. O. Abdulsalami, O.G. Fadodun, I.A. Egunjobi, Determination of optical parameters of zinc oxide nanofibre deposited by electrospinning technique, J. Taibah Univ. Sci. 11 (2017) 1245–1258, https://doi.org/10.1016/j.jtusci.2017.01.004.

[61] J.I. Pankove, Optical Processes in Semiconductors, Dover Publications Inc., New York, 1975, p. 91.

[62] J.S. Licurgo, G.R. de Almeida Neto, H.R. Paes Junior, Structural, electrical and optical properties of copper-doped zinc oxide films deposited by spray pyrolysis, Cerâmica 66 (2020) 379.

[63] V.K. Sabhapathi, O.M. Hussain, S. Uthanna, B.S. Naidu, P.J. Reddy, C. Julien, M. Balkanski, A.c. conductivity studies on Al/MoO3/Al sandwich structures, *Mater. Sci. Eng.*, B 32 (1995) 93–97, https://doi.org/10.1016/0921-5107(94)01173-7.

[64] G. Shanmuganathan, I.B. Shameem-Banu, S. Krishnan, B. Ranganathan, Influence of K-doping on the optical properties of ZnO thin films grown by chemical bath deposition method, J. Alloys Compd. 562 (15) (2013) 187–193.

[65] V. Sunke, U. Suda, Structural and optical properties of thermally oxidized zirconium dioxide films, Int. Lett. Chem. Phys. Astron. 77 (2017) 15–258.

[66] Y. Caglar, S. Ilican, M. Caglar, Single-oscillator model and determination of optical constants of spray pyrolyzed amorphous SnO_2 thin films, Eur. Phys. J. B. 58 (2007) 251–256.

[67] A.S. Hassanien, Studies on dielectric properties, optoelectrical parameters and electronic polarizability of thermally evaporated amorphous Cd50S50-xSex thin films, J. Alloys Compd. 671 (2016) 566–578.

[68] S. Thirumavalavan, K. Mani, S. Sagadevan, Investigation of the Structural, optical and electrical properties of Copper Selenide thin films, Cerâmica 66 (2020) 379, 10.1590/0366- 69132020663792877.

[69] L.M. Pereira, J.P. Araújo, U. Wahl, S. Decoster, M.J. Van Bael, K. Temst, A. Vantomme, Searching for room temperature ferromagnetism in transition metal implanted ZnO and GaN, J. Appl. Phys. 113 (2013), 023903.

[70] T. Maruyama, Y. Shiota, T. Nozaki, K. Ohta, N. Toda, M. Mizuguchi, Large voltage-induced magnetic anisotropy change in a few atomic layers of iron, Nat. Nanotechnol. 4 (2009) 158–161, https://doi.org/10.1038/nnano.2008.406.

[71] C.G. Duan, J.P. Velev, R.F. Sabirianov, Z. Zhu, J. Chu, S.S. Jaswal, Surface magnetoelectric effect in ferromagnetic metal films, Phys. Rev. Lett. 101 (2008) 137201, 10.1103/Phys Rev.Lett.101.137201.

[72] K. Nakamura, R. Shimabukuro, Y. Fujiwara, T. AkiyamaIto, A.J. Freeman, Giant modification of the magnetocrystalline anisotropy in transition-metal monolayers by an external electric field, Phys. Rev. Lett. 102 (2009) 187201, 10.1103/Phys Rev.Lett.102.187201.

[73] K. Nakamura, T. Akiyama, T. Ito, M. Weinert, A.J. Freeman, Role of an interfacial FeO layer in the electric-field-driven switching of magnetocrystalline anisotropy at the Fe/MgO interface", Phys. Rev. B 81 (2010) 220409, https://doi.org/10.1103/Phys.Rev.B.81.220409 (R).

[74] N. Madubuonu, S. Aisida, A. Ali, I. Ahmed, T. Zhao, S. Botha, M. Maaza, F. Ezema, Biosynthesis of iron oxide nanoparticles via a composite of *Psidium guavaja Moringa oleifera* and their antibacterial and photocatalytic study, J. Photochem. Photobiol. B Biol. 199 (2019) 111601, https://doi.org/10.1016/j.jphotobiol.2019.111601.

[75] J.D. Watts, L. O'Brien, J.S. Jeong, K.A. Mkhoyan, P.A. Crowell, C. Leighton, Magnetic impurities as the origin of the variability in spin relaxation rates in Cu-based spin transport devices, Phys. Rev. Mater. 3 (2019) 124409.

[76] S. Kumara, P. Mandal, A. Singh, S. Husain, D. Kumar, V.K. Malik, S. Sharma, Magnetization properties of Co incorporated ZnS nanocrystals synthesized at low temperature via chemical route, J. Alloys Compd. 830 (2020) 154640.

[77] A.H. Shah, M. Basheer Ahamed, E. Manikandan, R. Chandramohan, M. Iydroose, Magnetic, optical and structural studies on Ag doped ZnO nanoparticles, J. Mater. Sci. Mater. *Electron.* 24 (2013) 2302–2308, https://doi.org/10.1007/s10854-013-1093-6.

[78] N. Gopalakrishan, L. Balakrishan, A. Brindha, G. Jayalakshim, Thickness and substrate orientation dependence of ferromagnetism in Mn doped ZnO thin films, Cryst. Res. Technol. 47 (2011) 45–52, https://doi.org/10.1002/crat.201100425.